

# Experimental Analysis of the MRF Algorithm for Segmentation of Noisy Medical Images

Dorit S. Hochbaum, Joe Qranfal and Germain Tanoh

Volume 6, Number 2, Fall 2011

URI: [https://id.erudit.org/iderudit/aor6\\_2art02](https://id.erudit.org/iderudit/aor6_2art02)

[See table of contents](#)

Publisher(s)

Preeminent Academic Facets Inc.

ISSN

1718-3235 (digital)

[Explore this journal](#)

Cite this article

Hochbaum, D. S., Qranfal, J. & Tanoh, G. (2011). Experimental Analysis of the MRF Algorithm for Segmentation of Noisy Medical Images. *Algorithmic Operations Research*, 6(2), 79–90.

Article abstract

We show here that the implementation of the Markov random fields image segmentation algorithm of Hochbaum 2001 works well for the purpose of denoising and segmenting medical images. One of the main contributions here is the ability for a user to manipulate online the image so as to achieve clear delineation of objects of interest in the image. This is made possible by the efficiency of the implementation. Results are presented for images that are generated by Single Photon Emission Computed Tomography and Magnetic Resonance Imaging. The results show that the method presented is effective at denoising medical images as well as segmenting tissue types, organs, lesions, and other features within medical images. We advocate that this method should be considered as part of the medical imaging toolbox.



# Experimental Analysis of the MRF Algorithm for Segmentation of Noisy Medical Images

Dorit S. Hochbaum<sup>1</sup>

Department of Industrial Engineering and Operations Research and Walter A. Haas School of Business, University of California, Berkeley, USA

Joe Qranfal

Department of Mathematics, Simon Fraser University, Burnaby, BC, Canada

Germain Tanoh

Quantimal Consulting, Vancouver, BC, Canada

## Abstract

We show here that the implementation of the Markov random fields image segmentation algorithm of Hochbaum 2001 works well for the purpose of denoising and segmenting medical images. One of the main contributions here is the ability for a user to manipulate online the image so as to achieve clear delineation of objects of interest in the image. This is made possible by the efficiency of the implementation. Results are presented for images that are generated by Single Photon Emission Computed Tomography and Magnetic Resonance Imaging. The results show that the method presented is effective at denoising medical images as well as segmenting tissue types, organs, lesions, and other features within medical images. We advocate that this method should be considered as part of the medical imaging toolbox.

## 1. Introduction

The Markov random fields (MRF) model is well known in the image segmentation field. The MRF model is based on finding uniform color areas within images. The model tries to minimize any changes in color of pixels between the input and the output, while at the same time minimizing the difference in color between adjacent pixels in the output. In 2001, an efficient algorithm based on discrete optimization was developed for the convex case of the MRF model [16]. We use this algorithm for the purpose of denoising medical images. The software used to implement the algorithm for the MRF model is the most efficient algorithm for flow in practice, the pseudoflow algorithm [18]. The efficient implementation of the MRF model permits the user to adjust the input parameters and quickly receives feedback. The user thus receives feedback on the effect

of parameter changes almost instantly and effectively selects the parameters that give the best output image. Here we apply the MRF model to the medical imaging problem described next.

### 1.1. The Medical Imaging Problem

Recent advances in high-speed computing and image processing have contributed significantly to the progress of treatment planning including radiation therapy, hyperthermia, surgical procedures, and cryosurgery. The mathematical foundation of image formation and acquisition in biomedicine has been extensively studied [11,23,31,26,39]. Data is collected from a body exposed to radiation in this widely used physical process. There exist different categories of *imaging systems* or *modalities* [23,31]. The first radiology image was obtained by *X-ray computed tomography* and belongs to the family of *transmission tomography* imaging modality where the radiation source is outside the patient. Conversely with *emission tomography*, as in Positron Emission Tomography (PET) or in Single Photon Emission Computed Tomography (SPECT), the

*Email:* Dorit S. Hochbaum [hochbaum@ieor.berkeley.edu], Joe Qranfal [jqranfal@irmacs.sfu.ca], Germain Tanoh [tanoh@rocketmail.com].

<sup>1</sup> Research supported in part by NSF award No. DMI-0620677 and CBET-0736232.

radiation source is inside the patient. Magnetic resonance imaging (MRI), also known as nuclear magnetic resonance (NMR), has received much attention this last decade [31]. The object to be imaged is itself a signal source and is a function of the density of spins in the tissue. Some techniques provide information about the density of tissue, such as X-ray computed tomography, ultrasound CT [39], and MRI. Some others, like SPECT imaging, reflect physiology and biochemical function of a living organism. The raw data is acquired using physical instruments in all the imaging modalities. Then, a mathematical operation called *reconstruction* [6,32,7] is performed on this data in order to generate an image, which can be used for diagnostic purposes by a physician.

There exist two classes of tomographic reconstruction methods. The first class is composed of deterministic methods like convolution techniques, Fourier techniques, analytic methods, and iterative algebraic methods [32,26]. The second class comprises stochastic methods based on Bayesian analysis; the most well-known of these is the expectation maximization (EM) method [28,20,37]. The Kalman filtering approach belongs to this class of stochastic reconstruction techniques and is well-suited for dynamic SPECT image reconstruction [35,36]. However, sometimes the data recorded may not yield a unique solution, or the solution may not even exist at all. This phenomenon is exacerbated by physical degradation like camera blurring, photon scattering, or attenuation. Thus, the efficiency of a reconstruction method depends on its capability to remove the effect of the source of degradation, which is associated with the imaging system. Many studies have been carried out to stabilize the reconstruction algorithm against the effects of the physical degradation of the image through the incorporation of prior information about the image [24,15].

Another important aspect of medical image processing is the ability to focus or visualize important features of the image. For instance, quantitative information on tumor volume can help evaluate the efficacy of different treatments [34,40,31,14]. Thus we need mathematical methods to extract clinically important features from large data sets.

In the context of medical imaging, *segmentation* is an image analysis technique used to highlight a particular characteristic, organ, or object from the image data for visualization and measurement purposes; see for in-

stance [31]. Segmentation is the practice of classifying pixels into different object classes according to their spatial position, intensity, neighborhood, and/or prior knowledge about the object class. Segmentation plays a leading role in image analysis since it is a prerequisite step in most of the analysis, methods such as area and volume estimation, image co-registration, and motion detection.

The challenge presented by segmentation is finding a logical rule that produces efficient partition with as little human interaction as possible. In most cases, the problem is formulated as an optimization problem, where the objective function to be minimized is some energy function. In the celebrated paper of Geman and Geman [13], a stochastic based energy function was investigated. A more general model was proposed by Mumford and Shah [30]. These works gave rise to important mathematically challenging problems in image analysis [29,16]; see also the recent monograph of Chan and Shen [8] and references therein.

The most common segmentation methods are thresholding, region growing, classifiers, clustering, Markov random fields models, artificial neural networks, deformable models, and atlas-guided methods. Global thresholding is effective where sets of pixels associated with a physical property (e.g. an organ) clearly fall into distinct groups of colors within the image. However, this does not work well for low contrast segmentations, such as separating heart muscle from chest tissues or cerebral gray matter from white matter. Edge detection is difficult in medical images because the difference in intensities between the structure of interest and the surrounding structure can vary along the edge of the structure. Segmentation of medical images is an active research area; interested readers are referred to [34,40] and references therein, for a thorough survey on the subject.

## 1.2. Image Segmentation as Markov Random Fields Problem

The image segmentation problem is to partition a given digital image into multiple regions based on some criterion. We are given an image made up of pixels, each associated with a color or *intensity*. This given input image, referred to hereafter as the *observed* image, is a noisy representation of an *original* image, which is a perfect representation of the object. The noise may be caused either by information loss during transmission

or by inaccurate measurements as is the case in medical imaging [34]. The objective is to reset the values of pixel intensities to generate a *corrected* image. The methods used to generate a corrected image are based on the assumption that such an image tends to have uniform color areas, or segments. Each color area corresponds to what is presumed to be a distinct object in the image.

The *Markov random fields image segmentation* (MRF) problem considers an observed image. Each pixel in the image has a color and a set of pixels which are defined as the neighbors of the pixel. The objective is to generate a corrected image, whereby the values of its pixels minimize the sum of two penalties: These two components of the penalty function are defined as:

- (1) The cost of deviation of the pixel intensities of the corrected image from those of the observed image, called the *deviation cost*. The purpose of this cost function is to penalize differences from the observed image.
- (2) The cost of discontinuity in the corrected image penalizes the difference of the intensities of two neighboring pixels. This penalty function is called the *separation cost*. The purpose of the separation cost is to achieve uniform color areas and remove noise in the corrected image.

Thus the choice of colors assigned to pixels of the corrected image minimizes the penalty function consisting of the deviation penalties from the observed color shade and the separation penalties of differences in assigned values between neighboring pixels in the corrected image.

This problem has been studied over the past two decades, see e.g. [2], [3], [21], [12], [13]. MRF was addressed (prior to [16]) with two solution methods. The first method was to use heuristic and approximation approaches. The drawback of this approach is that the solution found is not optimal. The second method used to solve the MRF problem is with an optimal algorithm that does not work in polynomial time [21]. Rather, it creates multiple copies of the image graph, one for each possible label. The drawback of this approach is that the run time increases excessively with the number of labels. This makes it impractical for many situations. The method presented in this paper does not suffer either shortcoming.

We are given an observed image which is a set of pixels  $P$ , with a real-valued intensity  $r_i$  for each pixel  $i \in P$ . The *neighborhood* of pixel  $i$ , which contains

pixels we define as adjacent to  $i$ , is denoted by  $\mathcal{N}(i)$ . We wish to assign each pixel  $i \in P$  an intensity  $x_i$  that belongs to a discrete finite set  $X = \{\lambda_1, \lambda_2, \dots, \lambda_k\}$  so that the sum over all pixels of the deviation cost  $F_i(\cdot)$  and the separation cost  $G_{ij}(\cdot)$  is minimized. The MRF problem is formulated as follows:

(MRF)

$$\text{Minimize } D \sum_{i \in P} F_i(x_i) + S \sum_{i \in P} \sum_{j \in \mathcal{N}(i)} G_{ij}(x_i, x_j)$$

Subject To  $x_i \in X \quad \forall i \in P$

Once the penalty functions,  $F_i(\cdot)$  and  $G_{ij}(\cdot)$  are selected, an equal weighting of them may not produce a segmentation of adequate quality. When the separation function is more dominant, a higher importance is placed on the continuity of structures within the output, and in fact when the separation function overwhelms the deviation function, the output will become a single intensity. When the deviation function is more dominant, a higher emphasis is placed on keeping the pixel intensities close to the intensities in the input. If the deviation function completely overwhelms the separation function, the output image is simply the observed image mapped to the intensity values in  $X$ .

For this reason the positive integer coefficients  $S$  and  $D$  are added to the objective function and left to the control of the user to adjust the tradeoff between the deviation and separation penalties. Note that in fact only the ratio between  $S$  and  $D$  affects the segmentation. We define that ratio to be  $\gamma = \frac{S}{D}$  which can take on any nonnegative rational value.  $\gamma$  is varied until a corrected image of adequate quality, if one exists, is found. Our experience indicates that the values of  $\gamma$  for which adequate segmentations are produced are limited in any given application to a reasonable range of values, as we discuss in Section 3.3.1.

## 2. Implementation

Hochbaum [16] described the first known polynomial time algorithm for the MRF problem with convex separation and deviation functions. We refer to this implementation as the **MRF algorithm**. An important special case of the problem has any convex deviation function and linear separation functions – linear for positive separation and linear for negative separation. Thus penalties can be different for positive and negative separations. We chose here a specific setting of the penalty

functions in which  $F_i(\cdot)$  is convex quadratic:

$$F_i(x_i) = (x_i - r_i)^2$$

$$G_{ij}(x_i, x_j) = \begin{cases} \alpha_{ij}(x_i - x_j) & \text{if } x_i - x_j \geq 0 \\ \beta_{ij}(x_j - x_i) & \text{if } x_j - x_i > 0 \end{cases}$$

for  $\alpha_{ij}, \beta_{ij} > 0$ .

The optimal solution for the MRF algorithm with these penalty functions is achieved by reducing it to a parametric minimum cut problem on a constructed graph with  $k$  parameters as shown in [16]. The interested reader is referred to Hochbaum [16] and Hochbaum and Queyranne [19] for details of this approach.

The particular choice of the separation and deviation functions was made as specified because the functions are simple and this is not dominated by other choices. Although the convex MRF allows for any choice of convex functions we found that selecting other convex functions does not improve the segmentation. In fact choosing higher degree polynomial functions can cause too high penalty for larger deviations and may lead to too much uniformity in the output image without the ability to fine tune it. That is because small separations translate to very high penalties for higher degree polynomials. We found that the best control of the segmentation is afforded with the choice specified and using the  $\gamma$  ratio as the main mechanism for controlling the segmentation.

Generally, the neighbors of a pixel can be defined as being the four pixels horizontally and vertically adjacent to the pixel that form a cross around it. An eight pixel neighborhood includes those that are horizontally, vertically, and diagonally adjacent covering a nine pixel square with the original pixel in the center. The algorithm may be easily extended to three-dimensional segmentations by defining the pixel’s neighbors in all three dimensions. Pixels in a three-dimensional segmentation can be defined as having 6 or 18 neighbors.

The MRF algorithm is implemented using the highest label pseudoflow algorithm which was developed to solve the parametric maximum flow problem. The latest version of the pseudoflow algorithm code is available at [9].

While future research is needed to fine-tune our approach in order to apply it effectively to other cases, we have developed here an implementation that produces good quality images for our example problems. The implementation is fast, finding the solution to a  $256 \times 256$  pixel image in 3.4 seconds with a 2.0 Ghz Intel Core 2

processor. This efficiency permits the user to adjust the parameters of the MRF algorithm in real time and receive online feedback. Importantly, this means that the medical imaging operator could actively adjust a dial or other control mechanism to rapidly find the most acceptable segmentation, and hence the clearest image of the object.

### 2.1. Parameters Affecting Results

The task is to adjust the parameters so the corrected image is sufficiently close to the original. The definition of “close” is intentionally left ambiguous since this depends on the specific application. For most imaging applications, the closeness of the corrected image to the original is based purely on a qualitative visual assessment, but we have also used an error measurement. We have observed that the output of the algorithm depends significantly on two things: the value of  $\gamma$  and the choice of which and how many pixel intensities are included in the output.

An appropriate value for  $\gamma$  is chosen for each application of the MRF algorithm. We demonstrate that one can easily find values of  $\gamma$  to generate good corrected images using our technique. An analysis of the error between the output image and the true image as the value of  $\gamma$  varies is presented in Section 3.3.1..

The choice of the set of intensities that may appear in the output image,  $X = \{\lambda_1, \lambda_2, \dots, \lambda_k\}$ , has an effect on the quality of the segmentation results. The values of the set  $X$  may be taken from the original image, if available, or from sample images in a database to which the observed image can be compared. Although it can be challenging to find the ideal set  $X$ , once found it can be used in other images of the same type.

In many medical applications, the cardinality of the set  $X$  is known [34]: for example, the image may constitute three types of tissue. The cardinality of  $X$  is denoted by  $k = |X|$ . If no prior information is available about the set  $X$ , the values may be estimated from the observed image, given the value  $k$ . It is important to note that  $k$  is the number of values that *may* appear in the corrected image, not the number of values that *will* appear in the corrected image. For example, if the observed image consists entirely of one color, then the corrected image will be an image consisting of a single color as well – whichever color in the set  $X$  that is closest to the color in the observed image. It is easy to see that this is the case by assuming that a corrected



image,  $Img_i$ , contains more than one color whereas the observed image contains only one color. If this is compared to an image,  $Img_j$ , consisting only of the color in  $Img_i$  that is closest to the color in the observed image, then the total deviation penalties for  $Img_j$  will be less than or equal to the total deviation penalties for  $Img_i$ . Additionally, wherever pixels of different colors are neighbors, there will be a separation penalty for  $Img_i$ . Since the total penalties for  $Img_i$  will be strictly greater than  $Img_j$ ,  $Img_i$  cannot be the optimal segmentation and it is shown that when the observed image is a single color, the corrected image must be as well.

In this implementation, the default is to select the values of the set  $X$  from the observed image using a simple k-means procedure [27]. The set of values selected by this method is referred to here as the  $k$ -set. The advantages of the k-means algorithm are that it is very efficient and it finds a good approximation of the most common values in the observed image. The disadvantages are that it is a heuristic and the value of an area of interest (for example a lesion) may be small and therefore not likely to be selected by k-means. To compensate for these disadvantages, the implementation allows a value that is found to give good results in one k-set to be forced into other k-sets. The algorithm also allows the user to choose the values of the set  $X$  based on prior knowledge, without the use of k-means.

### 3. Results and Evaluation

The MRF algorithm can be applied to a multi-band image such as a color image or an image composed of multiple feature layers. However, all results presented here are single-band images. This section presents several experiments on selected applications from simple models to more realistic magnetic resonance brain images.

#### 3.1. Contaminated Noisy Images

In order to demonstrate the effectiveness of the MRF algorithm for medical imaging, we test it on noisy synthetic data. We take an original image and add to it noise to obtain what we refer to as a noisy “observed” image. The goal is to recover an image as close as possible to the original in terms of objects of interest by applying the MRF algorithm to the observed image. Figure 1 shows the original  $256 \times 256$  pixel image composed of a gray ring, a white disk and the background. We use

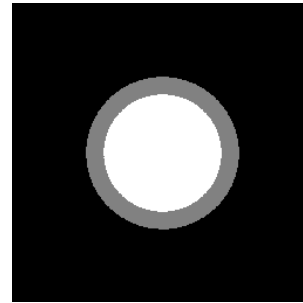


Fig. 1. Original image composed of a gray ring, a white disk and a black background.

different levels of signal-to-noise-ratio (SNR) and different levels of contrast-to-noise-ratio (CNR) to simulate an observed image contaminated by noise. Noise is added using Gaussian distributions for the white and grey regions and using Rayleigh distributions for the background. The first data set contains three images with decreasing CNR (Figure 2), and the second is a set of two images having different levels of SNR (Figure 3).

Figures 2 and 3 each present observed images with simulated noise in the top row. The bottom row of figures 2 and 3 display is the corrected images resulting from running the MRF algorithm on the respective observed image above. In these corrected images, the noise is totally removed so that the most important components are more visible and are very close to the original image. As expected, a higher CNR or SNR results in a better segmentation. Overall, the restored images capture the main features of the original image. We notice that the three regions (the white circle, the grey ring and the background) look well delineated compared to the original in Figure 3.1.. This is especially seen in Figure 2 (f) where the low level of CNR does not affect the performance of the algorithm. In Figure 2 from (d) to (e) to (f), the color of the background in the corrected image becomes lighter, and all three are lighter than in the original image in Figure 1 due to the selection of gray level by k-means. The added noise reduces the number of pixels with the intensity of the original background, causing the k-means algorithm to choose lighter colors for the image. The colors selected by k-means is not inherently inferior to using the colors in the original image. For example the segmentation, using k-means, of Figure 2 (c) as shown in Figure 2 (f) produces very good results, but when the colors from the original image are used, the segmentation is signifi-

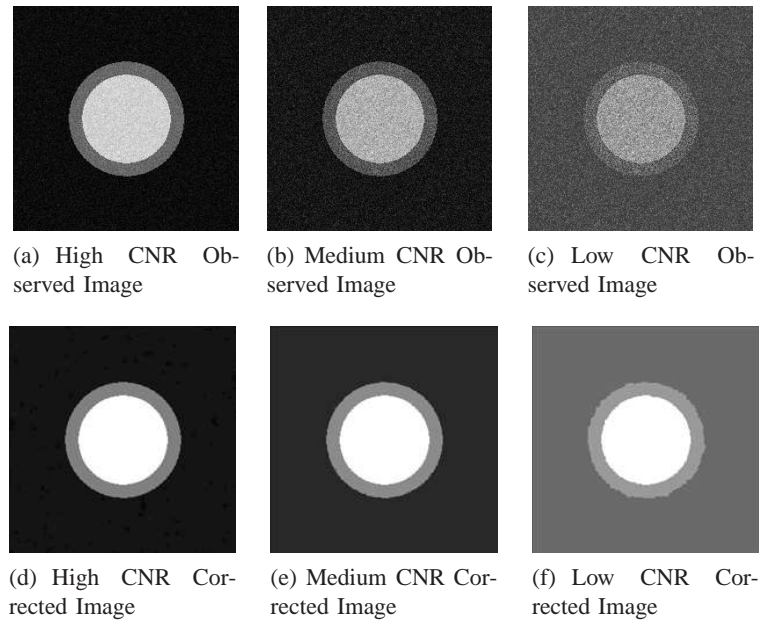


Fig. 2. First row: (a)-(c) from left to right, observed images with decreasing CNR. Second row: (d)-(f) from left to right, results of the segmentation of corresponding images.

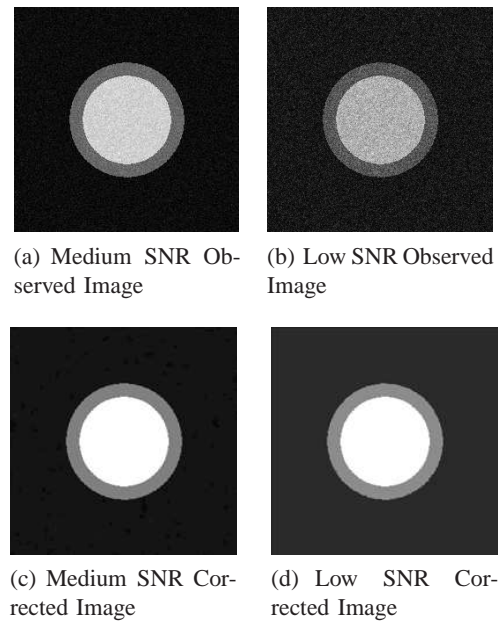


Fig. 3. First row: (a)-(b) from left to right, observed images with decreasing CNR. Second row: (c)-(d) from left to right, results of the segmentation of corresponding images.

cantly worse with the grey band and background merged into a single grey segment.

Most importantly, these examples demonstrate that the MRF Algorithm is able to find contours, which is necessary in medical imaging to separate the organ from the background. This confirms that the technique is well suited to enhance the quality of an image with poor spatial resolution and SNR such as encountered in SPECT imaging.

### 3.2. Segmentation of SPECT Images

In this section we assess these abilities using one slice of a digital thorax phantom. A SPECT image was simulated using the MCAT Phantom [33]. SPECT imaging informs us about the bio-distribution of specific radio-tracers. It is used in nuclear medicine for the diagnosis of abnormalities in a biochemical process. Unfortunately, SPECT images are inherently noisy and provide less quantitative information about the qualitative features discerned by the experienced observer.

Figure 4 shows the original image and the observed image using a SPECT imaging modality. This image represents a slice of a human chest and shows the liver, the lungs, the left and the right ventricle, and a defect in the heart, all surrounded by a background. Figure 5 shows the segmentation results of the reconstructed image using several  $k$ -sets for different values of the parameter  $k$  in the algorithm. The segmentation distinguishes different classes of region according to their intensities. It removes noise and the images are smoother. As a consequence, important features are highlighted (heart, liver and lungs). As the value of  $k$  is varied from 3 to 10, we notice that for smaller values of  $k$ , the segmentation result can omit some features in the original image. For  $k = 3$ , the left and the right ventricles and the lungs merge to form a single organ; however, the liver is well delineated. The later feature is less preserved with  $k$  greater than 4; nevertheless, the lesion starts to be seen.

The segmentation with  $k = 7$  is much better as it is able to distinguish the lesion and the liver does not lose its homogeneity. With  $k = 9$  and  $k = 10$ , almost all the regions are perfectly delimited and the lesion is visualized, but not as accurately as with  $k = 7$  or  $k = 8$ . The variation in features segmented is a result of the different  $k$ -sets chosen by the  $k$ -means algorithm for different values of  $k$ . As demonstrated by all these numerical experiments, the MRF algorithm is a powerful

tool for post-reconstruction smoothing to improve the visual quality of a SPECT image.

### 3.3. Application to Magnetic Resonance Image Segmentation

The experiment with the synthetic data demonstrated the success and the quality of the segmentation on an image having distinct and well-separated bands of pixels. We now validate the practicality of the segmentation algorithm with a more realistic object. We use T1 modality MR brain phantom images obtained from the brain Web Simulated Database at the McConnell Brain Imaging Center of the Montreal Neurological Institute, McGill University [10]. Figure 6 (a) represents one slice of a brain image affected by Multiple Sclerosis (MS) lesion. The brain is composed of different constituents or segments. The most representative are the cerebrospinal fluid (CSF), the gray matter (GM), the white matter (WM), the fat, the muscle & skin, skin, skull, glial matter, connective, MS Lesion and the background. We focused on the capability of the algorithm to isolate the CSF, GM, WM, and the MS lesion.

Multiple sclerosis is a disease that affects the central nervous system. Magnetic resonance imaging is used to monitor and assess the progression of the disease and to evaluate the effect of drug therapy. Clinical analysis of MS lesions is usually performed manually and suffers from lack of accuracy. The ability of an automatic segmentation to rapidly and accurately segment the MS lesions allows quantitative analysis of the disease and improves the accuracy of the evaluation.

In the brain MRIs which were segmented using the MRF algorithm, the number of colors,  $k$ , was set to 12 based on our prior knowledge of the brain anatomy: there are 11 kinds of tissues plus the background. We have the same observation for the restored brain images as for the synthetic data described in Section 3.1., less noise in the observed image results in better segmentations. We only report here the results of a segmentation of the brain with one specific noise added. In Figure 6 a MR image is shown segmented by the MRF algorithm. The results show that the proposed method is capable of segmenting an image made up of several parts with complex interconnection. Despite the lack of difference between brain pixel intensities of various tissues, the algorithm distinguishes the WM, CSF, GW and the MS lesion. Depending on the choice of the deviation and separation parameters, the algorithm succeeds to a cer-





(a) Original image of an unhealthy myocardium (b) Observed SPECT image

Fig. 4. SPECT image reconstruction

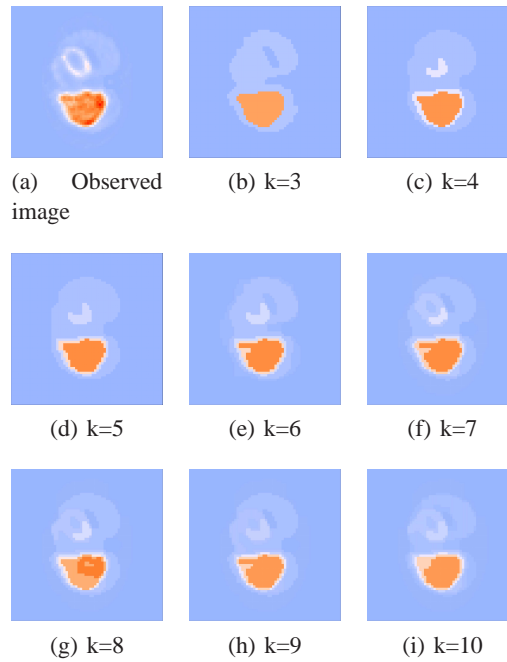


Fig. 5. Organ segmentation obtained with several k-sets for different values of  $k$ .

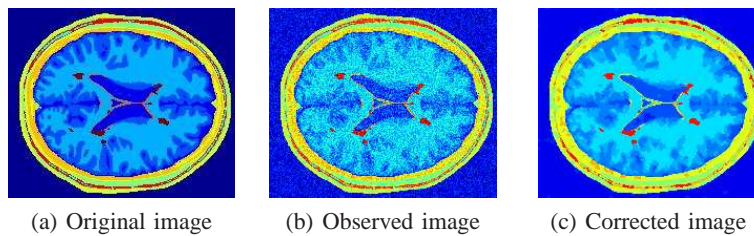


Fig. 6. Segmentation of Multiple Sclerosis brain image. (a) MS brain original image. The lesion are the red (brown) zone inside the brain. (b) Simulated observed MS Brain image, (c) Corrected MS brain image.

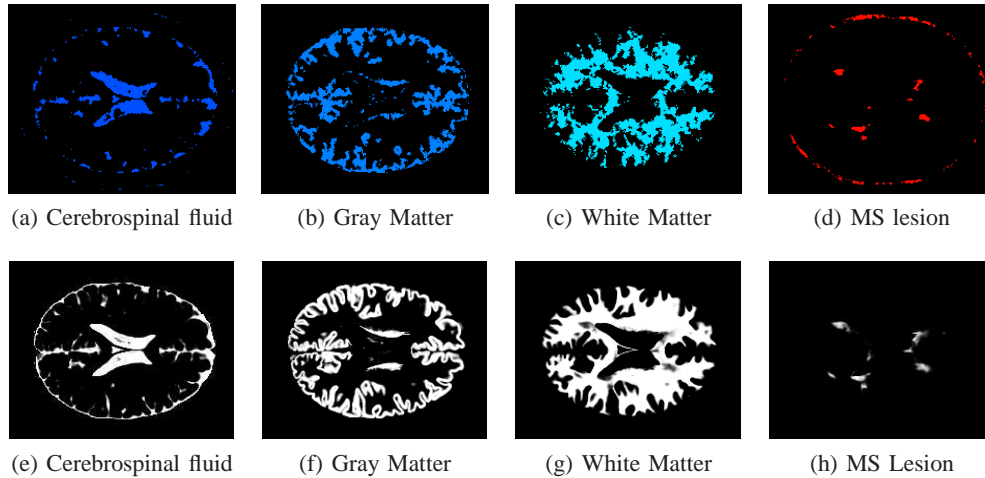


Fig. 7. Segmentation results of two brain images obtained with number of colors  $k = 12$ , deviation  $D = 2$  and separation  $S = 16$ . Sub figures (a) to (d) are, respectively, the segmented CSF, GM, WM and the MS lesion shown separately but segmented in the same image. (e)-(h) are the corresponding segments from the original image.

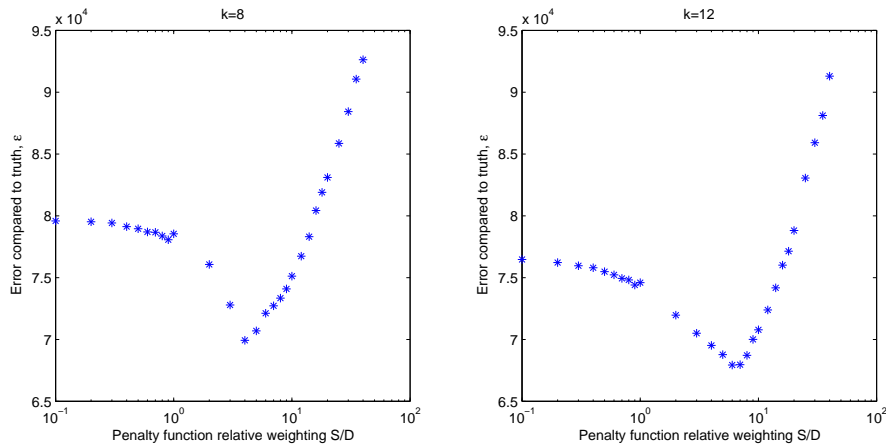


Fig. 8. Plot of the error between the corrected image and the original image as  $\gamma$  is varied. Left image, number of colors is  $k = 8$ . Right image, number of colors is  $k = 12$ .

tain extent to separate constituents of the brain image.

Figure 7 presents the original and corrected images shown in Figure 6 (a) and (c) in a different manner. Images (a) through (d) are the masked segments of Figure 6 (c) comprising the GM, WM, CSF and the MS lesion as well as the masked segmented of Figure 6 (a). A segment is masked in the sense it is the only one shown while the remaining segments are seen as a background. To ease then a visual comparison, each segment of Figure 6 (c) is shown separately from the rest of the corrected image, and beneath each corrected segment is

the corresponding segment from the original image of Figure 6 (a). Figure 7 (d) stresses the fact that the algorithm is able to identify the MS lesion, but can not perfectly isolate it from the rest of the tissues. This is a result of the lack of intensity difference between the Multiple Sclerosis(MS) lesion and other tissues, especially the WM. From a clinical viewpoint, this does not create undue confusion since we know that MS affects mainly the WM. We also emphasize the capability of the algorithm to segment while removing noise in order to highlight important features.

### 3.3.1. Quantitative Analysis

The forgoing analyses were based on visual inspection. We now include quantitative criteria to study the behavior of the separation-deviation segmentation with respect to  $\gamma$ , the ratio of  $S$  to  $D$ . Knowing the original image, we evaluate the quantitative performance by computing the relative error between the corrected images obtained as  $\gamma$  is varied and the original image. Let  $x^{orig}$  and  $x^{cor}$  be the original and the corrected images respectively, we denote by  $\varepsilon$  the error level computed as

$$\varepsilon = \|x^{orig} - x^{cor}\| = \sqrt{\sum_i^N (x_i^{orig} - x_i^{cor})^2},$$

where  $N$  is the total number of pixels in the image. As in the previous segmentations of brain MR images, the number of color values is set to  $k = 12$ , but we also present the error from a segmentation with  $k = 8$  for comparison. We evaluate the results by varying the value of  $\gamma = \frac{S}{D}$ . We are looking for a parameter  $\gamma$  for which the relative error  $\varepsilon$  as a function of  $\gamma$  is minimum. The plot in Figure 8 shows the experimental results of varying  $\gamma$ . The lowest error when  $k = 12$  is obtained when  $\gamma = 6$  and when  $k = 8$  is obtained when  $\gamma = 4$ . The plot provides an example of the importance of properly balancing the penalty functions for each type of application, as the error increases if either the separation or deviation function is allowed to dominate.

### 3.3.2. Discussion

The MRF algorithm performs well provided that the different classes of pixels are well separated in terms of intensity, as demonstrated with the synthetic dataset. Unfortunately this is not always true for MR images of the brain. Because of the limited spatial resolution of image modality and the complexity of the anatomic structure of some brain tissues, a single tissue voxel may be composed of several tissue types, which is called *partial volume* (PV) effect. An example of this is the lack of intensity difference between MS lesions and the other tissues of the brain. As a consequence, intensity similar to the lesion is found in several regions of the brain. As a remedy, a priori knowledge of the anatomical location of brain tissues can be used. In the current example, since most of the MS lesions are located in the white matter, one approach to improve the result is to confine the segmentation area. Exploiting the knowledge that the majority of MS lesion are located inside WM is a widespread technique in MR image segmentation [22,25].

The right number of color intensities,  $k$ , for a given data set is usually not known a priori. It can be automatically approximated using statistical techniques like Akaike Information Criterion (AIC) [1]. Once a satisfactory number of intensities is found, the deviation and the separation parameters,  $S$  and  $D$ , are tuned by the user online according to their preference. An interesting aspect that remains to be explored is the automatic estimation of the number of intensities simultaneously with the optimal deviation and separation ratio. This could be done using AIC as discussed above or Schwarz criterion [38], which are two ways to measure the goodness of fit of an estimated statistical model.

## 4. Conclusions

We demonstrate here an efficient implementation of an algorithm for the MRF problem applied to medical images. The results show that the MRF algorithm is effective at denoising medical images as well as segmenting tissue types, organs, lesions, and other features within medical images.

The MRF algorithm is highly efficient, meaning that results are produced so rapidly that a medical imaging operator could actively adjust input parameters to generate and select the most acceptable segmentation in almost real time interactively. It also means that the MRF algorithm may be used to deblur and segment very large images such as very high resolution images and 3-dimensional images.

We presented here corrected images generated by the MRF algorithm from synthetic images, SPECT images, and MRI images. The synthetic images demonstrated the ability of the algorithm to segment images with low signal-to-noise-ratios and low-contrast-to-noise ratios. The SPECT images showed that the algorithm is able to segment individual organs within images. The MRF algorithm also significantly increased the visibility of a lesion which is otherwise very difficult to see in the observed image.

The application of the algorithm to MRI images demonstrated the ability of the algorithm, not only to remove noise from the image, but also to effectively separate various tissue types. Most importantly, it can distinguish MS lesions within the noisy observed image.

The flexibility of the implementation of the MRF algorithm allows it to be used with other applications

in addition to those shown here, since the algorithm is modality independent. A challenging issue is to apply the MRF algorithm, for instance, in MRI segmentation to perform the segmentation of brain structures with some pathologies. Nevertheless, the MRF algorithm is efficient and effective for the segmentation of medical images. It can be applied to images for which other methods, such as global thresholding and edge detection, would not work. As such, it should be considered as part of the medical imaging toolbox.

### Acknowledgement

This is to thank Bala Chandran for his contributions on the software development and on running the initial experiments, and to Yao Ma and John Baumler for further software development and experimentations.

### References

- [1] H. Akaike. A new look at the statistical model identification. *IEEE Trans. Automatic Control*, 19(1974), 716–723.
- [2] Blake A. and Zisserman A. *Visual reconstruction*. MIT Press. 1987.
- [3] Boykov Y., Veksler O. and Zabih R. Markov Random fields with efficient approximations. In *Proc IEEE conference CVPR Santa Barbara CA*, (1998) 648–655.
- [4] Boykov Y., Veksler O. and Zabih R. Fast approximate energy minimization via graph cuts. *Proc 7th IEEE International Conference on Computer Vision*, (1999) 377–384.
- [5] Y. Boykov and V. Kolmogorov. An Experimental Comparison of Min-Cut/Max-Flow Algorithms for Energy Minimization in Vision. *IEEE transactions on Pattern Analysis and Machine Intelligence (PAMI)*, 26(2004), 1124–1137.
- [6] P. P. Bruyant. Analytic and iterative reconstruction algorithms. *SPECT, The Journal of Nuclear Medicine*, 43(2002) 1343–1358.
- [7] C. Byrne. Iterative algorithms in tomography. <http://faculty.uml.edu/cbyrne/nlat.pdf>. 2005.
- [8] T. F. Chan and J. Shen. *Image processing and analysis*. SIAM, Philadelphia. 2005.
- [9] B. G. Chandran and D. S. Hochbaum. Pseudoflow solver, accessed January 2011. <http://riot.ieor.berkeley.edu/riot/Applications/Pseudoflow/>.
- [10] D. L. Collins, A. P. Zijdenbos, V. Kollokian, J. G. Sled, N. J. Kabani, C. J. Holmes, A. C. Evans. Design and Construction of a Realistic Digital Brain Phantom. *IEEE Transactions on Medical Imaging*, 17(1998) 463–468.
- [11] C. L. Epstein. *Introduction to the mathematics of medical imaging*, Pearson Education, Inc. 2003.
- [12] D. Geiger and F. Girosi. Parallel and deterministic algorithms for MRFs: surface reconstruction. *IEEE Transactions on Pattern Analysis and Machine Intelligence*, 13(1991) 401–412.
- [13] S. Geman and D. Geman. Stochastic relaxation, gibbs distributions and the bayesian restoration of images. *IEEE Transactions on Pattern Analysis and Machine Intelligence*, 6(1984) 721–741.
- [14] P. Gibbsy, D. L. Buckleyz, S. J. Blackbandz and A. Horsmanz. Tumour volume determination from MR images by morphological segmentation. *Phys. Med. Biol.* 41(1996) 2437–2446.
- [15] P. J. Green. Bayesian reconstruction from emission tomography data using a modified EM algorithm, *IEEE Trans. Med. Imaging*, 9(1990) 322–338.
- [16] D. S. Hochbaum. An efficient algorithm for image segmentation, Markov random fields and related problems. *Journal of the ACM*, 48(2001) 686–701.
- [17] D. S. Hochbaum. Selection, Provisioning, Shared Fixed Costs, Maximum Closure, and Implications on Algorithmic Methods Today. *Management Science*, 50(2004) 709–723.
- [18] D. S. Hochbaum. The Pseudoflow algorithm: A new algorithm for the maximum flow problem. *Operations Research*, 58(2008) 992–1009.
- [19] D. S. Hochbaum and M. Queyranne. Minimizing a convex cost closure set. *SIAM J. Discrete Math.*, 16(2003) 197–207.
- [20] H. M. Hudson and R. S. Larkin. Accelerated image reconstruction using ordered subset of projection data. *IEEE Trans. Med. Imag.*, 13(1994) 601–609.
- [21] H. Ishikawa and D. Geiger. Segmentation by Grouping Junctions. *IEEE Conference on Computer Vision and Pattern Recognition*, CVPR 98(1998), 125–131.
- [22] B. Johnston, M. S. Atkins, and B. Mackiewicz. Segmentation of multiple sclerosis lesions in intensity corrected multispectral MRI. *IEEE Trans. Med. Imaging*, 15(1996) 154–169.
- [23] A. Kak and M. Slaney. *Principles of Computerized Tomographic Imaging*. SIAM (2001), Philadelphia.
- [24] K. Lange. Convergence of EM Image Algorithms with Gibbs Reconstruction Smoothing. *IEEE Transactions On Medical Imaging*, 9(1990) 439–446.
- [25] , K. V. Leemput, F. Maes, D. Vandermeulen, A. Colchester, and P. Suetens. Automated segmentation of multiple sclerosis lesions by model outlier detection. *IEEE Trans. Med. Imaging*, 20(2001) 677–688.
- [26] A. K. Louis. Medical imaging: state of the art and future development. *Inverse Problems*, 8(1992) 709–738.
- [27] J. MacQueen. Some methods for classification and analysis of multi-variate observations. *Proc. of the Fifth Berkeley Symposium on Math., Statistics and Probability*, L. M. LeCam and J. Neyman eds. U. California Press, Berkeley. (1967) 281–297.

- [28] G. J. McLachlan and Krishnan. *The EM Algorithm and Extensions*. John Wiley and Sons 1997.
- [29] J. M. Morel and S. Solimini. *Variational methods in image segmentation*. Birkhäuser, Boston 1995.
- [30] D. Mumford and J. Shah. Boundary detection by minimizing functionals, I. *Proc. IEEE Conf. on Computer Vision and Pattern Recognition, San Francisco, CA* 1985.
- [31] National Academy of Sciences. *Mathematics and Physics of Emerging Biomedical Imaging* 1990.
- [32] F. Natterer and F. Wübbeling. *Mathematical Methods in Image Reconstruction* 2001.
- [33] P. H. Pretorius, M. A. King, B. M. W. Tsui, K. J. LaCroix, and W. Xia. A mathematical model of motion of the heart for use in generating source and attenuation maps for simulating emission imaging. *Med. Phys.*, 26(1999) 2323–2332.
- [34] D. L. Pham, C. Xu, and J. L. Prince. A survey of current methods in medical image segmentation. *Annual Review of Biomedical Engineering*, 2(2000) 315–337.
- [35] J. Qranfal. Optimal Recursive Estimation Techniques for Dynamic Medical Image Reconstruction. *Simon Fraser University*, Ph.D. Thesis 2009.
- [36] J. Qranfal and G. Tanoh. Regularized Kalman filtering for dynamic SPECT. *Journal of Physics: Conf. Ser.*, 124(2008), 012042.
- [37] A. J. Rockmore and A. Macovski. A Maximum Likelihood Approach to Emission Image Reconstruction from Projection. *IEEE Trans. Nucl. Sci.*, 23(1976) 1428–1432.
- [38] Schwarz, G. . Estimating the dimension of a model. *Ann. Stat.*, 6(1978) 461-464.
- [39] P. N. T. Wells. Ultrasound imaging. *Phys. Med. Biol.*, 51(2006), R83–R98.
- [40] O. Wirjadi. Survey of 3D image segmentation methods. *Technical Report*, 123, Fraunhofer ITWM, Kaiserslautern (2007).

---

Received 19-11-2010; revised 27-5-2011; accepted 21-6-2011